Analytical Model for Calculating the Nonlinear Distortion in Silicon-Based Electro-Optic Mach–Zehnder Modulators

Ana M. Gutierrez, Antione Brimont, Javier Herrera, Mariam Aamer, Dave J. Thomson, Frederic Y. Gardes, Graham T. Reed, Jean-Marc Fedeli, and Pablo Sanchis, *Member, IEEE*

***Abstract*—In this study, an analytical model for calculating the nonlinear harmonic/intermodulation distortion for RF signals in silicon-based electro-optic modulators is investigated by considering the nonlinearity on the effective index change curve with the operation point and the device structure simultaneously. Distortion expressions are obtained and theoretical results are presented showing that optimal modulator parameters can be found to linearize it. Moreover, the harmonic distortion of a 1 mm silicon-based asymmetric MZI is RF characterized and used to corroborate the theoretical results. Based on the present model, the nonlinear distortion in terms of bias voltage or operating wavelength is calculated and validated by comparing with the experimental data, showing a good agreement between measurements and theory. Analog photonic link quality parameter like carrier-to-distortion is one of the parameters that can be found with that model. Finally, the modulation depth is measured to assure that no over-modulation is produced.**

***Index Terms*—Electrooptic modulation, integrated optics, nonlinear distortion, silicon on insulator technology.**

I. Introduction

YEAR after year a gradual transition from electrical to optical technology is being carried out allowing much longer links with larger bandwidths. This transition arises from the increasing need to transfer the maximum amount of information with the least cost, increasing the complexity and requirements in the networks interconnects including on-chip and off-chip communications. Besides this gradual transition, recently, the distribution of analog radio frequency (RF) signals over the optical fibers is catching growing attention and compounding the called analog photonics links (APL). These links, in which an RF signal is converted to the optical domain, distributed via optical fiber and reconverted to electrical format, are the heart of the profitable field of microwave photonics. This technology encompasses numerous potentially rewarding applications such as radio-over-fiber (RoF), antenna remoting, subcarrier transmission, signal processing or photonic analog-to-digital conversion [1], [2].

On the other hand, on-chip integration of discrete photonic components is a longstanding goal of integrated optics. Silicon-on-insulator technology, that utilizes scalable CMOS technology, has turned out to be a suitable platform to reach impressive levels of integration of most high performance silicon photonics devices [3], [4]. So, the use of silicon photonic devices to generate and process analog RF signals may lead to chip-size reduction and power efficiency improvements. Among the numerous building blocks required to enable a fully functional photonic integrated chip along with high speed electronics, electro-optic modulators, which link the electrical and optical domain, are essential [5]. These are just the devices employed in APLs for converting the RF signals into the optical format and they are of paramount importance for achieving high performance links. The leading approach for developing electro-optical modulators in silicon photonics is currently via the plasma dispersion effect which consists of varying the free-carrier concentration in a doped silicon waveguide [6], [7]. The electro-optic mechanism achieved with the plasma dispersion is an inherent nonlinear effect. Moreover the cosine-squared Mach–Zehnder Interferometer (MZI) structure also shows a nonlinear transfer function. Therefore, the nonlinearity at the output of a silicon-based MZI modulator is originated basically from the operating bias point of the modulator nonlinear transfer function combined with the intrinsic nonlinear response of the material in the active area. These nonlinearities in the modulator create distortions which limit the performance of an APL, but also that can be exploited, for example using the electro-optic modulator as a photonic microwave mixer.

Significant milestones have been achieved during recent years through the plasma dispersion effect although mostly for digital applications [8]–[20], but so far very little attention has been

Manuscript received January 24, 2013; revised September 10, 2013; accepted October 16, 2013. Date of publication October 22, 2013; date of current version November 4, 2013. This work was supported by the funding from the European Commission under project HELIOS (pHotonics Electronics functional Integration on CMOS), FP7-224312. The work of P. Sanchis and J.-M. Fedeli was supported by the funding funding from TEC2012-38540 LEOMIS, TEC2008-06333 SINADEC, and PROMETEO-2010-087. The work of F. Y. Gardes, D. J. Thomson and G. T. Reed was supported by funding received from the UK EPSRC funding body under the grant "UK Silicon Photonics."

A. M. Gutierrez, A. Brimont, M. Aamer and P. Sanchis are with the Nanophotonics Technology Center (NTC), Universitat Politecnica Valencia, Valencia 46022, Spain (e-mail: angucam@ntc.upv.es; abrimont@ntc.upv.es; maaa@ntc.upv.es; pabsanki@ntc.upv.es).

J. Herrera is with Fibernova Systems, S. L., Universitat Politecnica Valencia, Valencia 46022, Spain (e-mail: jherrera@fibernova.com).

D. J. Thomson, F. Y. Gardes and G. T. Reed are with the Optoelectronics Research Centre, University of Southampton, Southampton SO17 1BJ, U.K. (e-mail: d.thomson@soton.ac.uk; f.gardes@soton.ac.uk; g.t.reed@soton.ac.uk).

J. M. Fedeli is with CEA, LETI, 38054 Grenoble, France (e-mail: jean-marc.fedeli@cea.fr).

Color versions of one or more of the figures in this paper are available online at http://ieeexplore.ieee.org.

Digital Object Identifier 10.1109/JLT.2013.2286838

paid to analog applications. As mentioned above, high linearity is required for RF signal transmission. In this case, the distortion terms closest to the frequency of the transmitted signal have to be reduced. A lot of methods to improve the commercial $LiNbO_3$ modulators linearity have been published, using linearization schemes based on pre- and post-compensation distortion [21]–[23]. In silicon, a modulator linearization scheme was reported in [24] showing a silicon-based modulator with superior linearity with respect to a conventional MZI modulator. Moreover, other silicon-based modulators have been used for RoF transmission allowing very high features such 50 dB [25] or 57 dB [26] carrier-to-distortion ratio, showing significant advantages for emerging RoF applications. In contrast with the plain analog signal transport, many nonlinear applications such as mixing or frequency conversion are proposed techniques in the microwave photonics field. In this case, the nonlinear operation of the modulator is exploited, taking advantage of the distortion produced by the nonlinearities. The objective in that case is to maximize the farthest distortion terms. Many works have been reported about these techniques [27]–[31] using commercial $LiNbO_3$ modulators. In silicon, we recently reported a photonic mixer with excellent quality parameters, such a 7 dB conversion losses and an error vector magnitude of 8%, for frequency conversion applications [32].

Thus, the investigation of the distortion properties of silicon modulators is an important question for future all silicon analog photonic applications. In [24], the modulator linearity is analyzed theoretically, using models and numerical simulations. However, the expressions presented are limited to a symmetric push-pull configuration which automatically cancels the second order and higher-order even terms of the phase response. Moreover, in [25], the measurements are verified by simulation results showing the same trend, but no analytical expressions are presented. In this study, we develop an analytic model for calculating the distortion of a silicon-based electro-optic MZI modulator by taking into account the nonlinearity on the effective index change with the bias operation point and the device's structure simultaneously. The modulator transfer function is expanded into a Taylor series obtaining the second (2^{nd}) and third (3^{rd}) order harmonic and intermodulation terms so the model allows the designer to set a proper choice of modulator parameters to linearize the device or to enhance the nonlinearities. Finally, the harmonic distortions are validated with experimental measurements of a fabricated silicon MZI modulator.

II. Analytical Model

The plasma dispersion effect, the most commonly adopted electro-optic effect in silicon, consists of a change in the silicon refractive index by varying electrons and holes distribution within the material. The induced real refractive index (Δn) produced by the free-carrier plasma dispersion effect at the wavelength of 1.55 μm is calculated as follows [7]:

$$\Delta n = \Delta n_e + \Delta n_h = -[8.8\times 10^{-22}\Delta N + 8.5\times 10^{-18}\Delta P^{0.8}] \tag{1}$$

where Δn_e and Δn_h are the refractive index changes due to electrons and holes concentration changes ΔN and ΔP (in cm^{-3}). Equation (1) indicates that the index change by the plasma dispersion is a nonlinear effect [6], [7]. This nonlinear dependency produces intermodulation and harmonic distortion terms. In contrast with linear material-based modulators such $LiNbO_3$, in which the distortion usually have the same performance with the bias point (at quadrature bias point, all even order distortion terms vanish, while odd order maximize), for a nonlinear material the distortion depends on several factors. So, this is the first motivation for the development of a model which can help to predict the distortion performance in a silicon-based modulator.

If the Δn index varies by plasma dispersion effect, there will be a change Δn_{eff} in effective index of the propagating mode. In general, Δn can be regarded as proportional to Δn_{eff}. Therefore, the injection of an electric field causes a change in the effective refractive index of the guided mode, which in turn induces a change in the accumulated phase in the propagation distance L_{ACT}:

$$\Delta\Phi = \frac{2\pi}{\lambda}\Delta n_{\mathrm{eff}} L_{\mathrm{ACT}} \tag{2}$$

where Δn_{eff} is the effective index change, λ is the wavelength, and L_{ACT} is the length of the active region. By embedding such optical phase modulation in an MZI structure, it is possible to convert the phase modulation into intensity modulation. The MZI transfer function between bias parameter, dc voltage or operating wavelength (in an asymmetric MZI structure), and optical output power is periodic with such bias parameter. This periodic function is a nonlinear cosine-squared, which also produces intermodulation and harmonic distortions.

Harmonic distortion can be defined as a single-tone distortion product caused by device nonlinearity. When a nonlinear device is stimulated by a signal at frequency f_1, spurious output signals can be generated at the harmonic frequencies $2f_1$, $3f_1$, $4f_1$, i.e., at Nf_1. The order of the distortion product is given by the N frequency multiplier. Intermodulation distortion is a multi-tone distortion product that results when two or more signals are present at the input of a nonlinear device. The second-order intermodulation products of two signals at f_1 and f_2 would occur at $f_1+f_2, f_2-f_1, 2f_1$ and $2f_2$ and third-order at $2f_1+f_2, 2f_1-f_2, f_1+2f_2$ and f_1-2f_2, that is, at $Nf_1 \pm f_2$ or $f_1 \pm Nf_2$ with $N=1$ for the second-order terms and $N=2$ for the third ones. Here and for the development of our model, we assume that the APL nonlinearity is dominated only by the modulation device. Thus, we assume that other devices in the APL, such us the photo-detector, are linear. These components also contribute to APL nonlinearities but generally their contributions are much smaller compared to that of the modulation devices [33] and, hence, most of the time can be neglected.

A. Model Derivation

The starting point of the model is the effective index change with the applied dc voltage. As we have already mentioned, this dependence is nonlinear for the silicon-based MZI. The nonlinear form of the effective index change can be approximated by

a logarithmic curve [25], [34] as shown in (3):

$$\Delta n_{\text{eff}} = k \ln\left(1 + \frac{V_{\text{app}}}{V_b}\right) \tag{3}$$

where k (dimensionless) and V_b (in volts) are constants. In our case, we will use these parameters to fit the curve with the dc performance experimental results of the effective index variation. This effective index change induces a phase shift that accomplishes (2). Furthermore, in case of having a length difference between two arms of the MZI also induces an additional phase shift proportional to this length difference. Thereupon, we can regard that the total induced phase shift is due to two factors: the device structure, related with modulator transfer function, which has been called $\Delta\Phi_{\text{Bias}}$ and allows driving the modulator to the appropriate operation bias point; and the silicon in the active area, which has been named as $\Delta\Phi_{\text{Si}}$, and it is described in (5). So, the final phase shift expression can be written as

$$\Delta\Phi_{\text{TOT}} = \Delta\Phi_{\text{Si}} + \Delta\Phi_{\text{Bias}} \tag{4}$$

where

$$\Delta\Phi_{\text{Si}} = \frac{2\pi}{\lambda}\Delta n_{\text{eff}} L_{\text{ACT}}. \tag{5}$$

Finally, the detected optical power at the output of a MZI modulator is:

$$P_{\text{out}} = P_{\text{in}} \cos^2\left(\frac{\Delta\Phi_{\text{TOT}}}{2}\right) \tag{6}$$

where P_{in} is the input optical power to the modulator. If we substitute the total phase shift described by (4) in (6) and expand the cosine, we can state the output power as

$$P_{\text{out}} = P_{\text{in}} \begin{pmatrix} \frac{1}{2} + \frac{1}{2}\cos\left(\Delta\Phi_{\text{Si}}\right)\cos\left(\Delta\Phi_{\text{Bias}}\right) \\ -\frac{1}{2}\sin\left(\Delta\Phi_{\text{Si}}\right)\sin\left(\Delta\Phi_{\text{Bias}}\right) \end{pmatrix}. \tag{7}$$

Also, the phase shift due to the silicon using the expressions (3) and (5) results:

$$\Delta\Phi_{\text{Si}} = \frac{2\pi}{\lambda} L_{\text{ACT}} \Delta n_{\text{eff}} = \sigma \ln\left(1 + \frac{V_{\text{app}}}{V_b}\right) \tag{8}$$

where we have defined the design parameter σ (in radians) as shown in (9):

$$\sigma = \frac{2\pi}{\lambda} L_{\text{ACT}} k. \tag{9}$$

On the other hand, in a two-tone test, the input signal takes the form:

$$V_{\text{rf}} = V_{\text{RF}_1}\cos\left(\omega_1 t\right) + V_{\text{RF}_2}\cos\left(\omega_2 t\right) \tag{10}$$

where V_{RF1} and V_{RF2} are the RF signals amplitudes and $\omega_1 = 2\pi f_1$ and $\omega_2 = 2\pi f_2$ are the angular modulating frequencies. So, finally, the total applied voltage to the electro-optic modulator is the sum of one dc term and one RF term, as:

$$V_{\text{app}} = V_{\text{DC}} + V_{\text{rf}} = V_{\text{DC}} + V_{\text{RF}_1}\cos(\omega_1 t) + V_{\text{RF}_2}\cos(\omega_2 t). \tag{11}$$

So, if we make a compilation of the above equations and we substitute each equation into each other, we realize that the final expression for the silicon phase shift results:

$$\Delta\Phi_{\text{Si}} = \sigma\left(Y_{\text{DC}} + \ln\left(1 + X_1\cos\left(\omega_1 t\right) + X_2\cos\left(\omega_2 t\right)\right)\right). \tag{12}$$

For simplicity, the model has been developed under the assumption that the two tone input signals are of equal amplitude and the small signal approximation $\text{V}_{\text{RF}} \ll \text{V}_{\text{b}}$, so:

$$X_1 = X_2 = X = \frac{V_{\text{RF}}}{V_b + V_{\text{DC}}} \ll 1. \tag{13}$$

Finally, we can write the silicon phase shift as described in (14):

$$\Delta\Phi_{\text{Si}} = \sigma\left(Y_{\text{DC}} + \ln\left(1 + Y\right)\right) \tag{14}$$

where Y and Y_{DC} are given by (15) and (16) respectively:

$$Y = X(\cos(\omega_1 t) + \cos(\omega_2 t)) \tag{15}$$

$$Y_{\text{DC}} = \ln\left(1 + \frac{V_{\text{DC}}}{V_b}\right). \tag{16}$$

Now, the silicon phase shift can be expanded into the natural logarithm Taylor series of ln(1 + *Y*). The result will consist of a dc component which does not depend on ω, and a set of harmonics and intermodulation distortion terms. Finally, the silicon phase shift resulted of this Taylor series is:

$$\Delta\Phi_{\text{Si}} = \sigma \begin{pmatrix} -\frac{1}{2}X^2 + \left(X + \frac{3}{4}X^3\right)\cos(\omega_1 t) \\ -\frac{1}{4}X^2\cos(2\omega_1 t) + \frac{1}{12}X^3\cos(3\omega_1 t) \\ -\frac{1}{2}X^2\cos((\omega_1 \pm \omega_2)t) + \frac{1}{4}X^3\cos((2\omega_1 \pm \omega_2)t) \end{pmatrix}. \tag{17}$$

Plugging this expression of the silicon phase shift into (7) and performing another Taylor expansion of the cosine and sine, the result is again a set of harmonic and intermodulation products. The amplitudes of all these components will be sums of linear combinations of X, Y_{DC} and σ. The desired expressions that describe the modulator amplitudes nonlinearities are finally obtained and described by (18) in which the sub-index 'c' is referring to cosine and 's' to sine:

$$\begin{aligned} P_{\text{FUND.}}(\omega_1) &= \begin{cases} \frac{1}{2}\cos(\Delta\Phi_{\text{Bias}})[\Phi_{\text{FUND}c}X] \\ -\frac{1}{2}\sin(\Delta\Phi_{\text{Bias}})[\Phi_{\text{FUND}s}X] \end{cases} \\ P_{\text{IMD2}}(\omega_1 \pm \omega_2) &= \begin{cases} \frac{1}{2}\cos(\Delta\Phi_{\text{Bias}})[\Phi_{\text{IMD2}c}X^2] \\ -\frac{1}{2}\sin(\Delta\Phi_{\text{Bias}})[\Phi_{\text{IMD2}s}X^2] \end{cases} \\ P_{\text{IMD3}}(2\omega_1 \pm \omega_2) &= \begin{cases} \frac{1}{2}\cos(\Delta\Phi_{\text{Bias}})[\Phi_{\text{IMD3}c}X^3] \\ -\frac{1}{2}\sin(\Delta\Phi_{\text{Bias}})[\Phi_{\text{IMD3}s}X^3] \end{cases} \end{aligned} \tag{18}$$

As we can observe, the fundamental, second-order and third-order amplitudes are the terms with linear, quadratic, and cubic dependence on the modulating signal V_{RF}, respectively. Finally,

the cosine phase expressions are:

$$\Phi_{\mathrm{FUND}c} = (-Y_{\mathrm{DC}})\sigma^2$$
$$\Phi_{\mathrm{IMD2}c} = \left(\frac{1}{2}Y_{\mathrm{DC}} - \frac{1}{2}\right)\sigma^2$$
$$\Phi_{\mathrm{IMD3}c} = \left(-\frac{1}{2}Y_{\mathrm{DC}} + \frac{3}{8}\right)\sigma^2. \quad (19)$$

And the sine phase expressions:

$$\Phi_{\mathrm{FUND}s} = \sigma - \left(\frac{1}{2}Y_{\mathrm{DC}}^2\right)\sigma^3$$
$$\Phi_{\mathrm{IMD2}s} = \left(-\frac{1}{2}\right)\sigma + \left(\frac{1}{4}Y_{\mathrm{DC}}^2 - \frac{1}{2}Y_{\mathrm{DC}}\right)\sigma^3$$
$$\Phi_{\mathrm{IMD3}s} = \left(\frac{1}{4}\right)\sigma - \left(\frac{1}{8}Y_{\mathrm{DC}}^2 - \frac{3}{8}Y_{\mathrm{DC}} + \frac{1}{8}\right)\sigma^3. \quad (20)$$

The IMD amplitudes differ from the HD amplitudes even though they are basically generated by the same mechanism. It has been found that the IMD2 amplitude is twice that of the HD2 amplitude while the IMD3 amplitude is three-times the HD3 amplitude. However, the powers of these components rather than the amplitudes are usually measured. If we regard the amplitude to be either a current or a voltage, then the power considered here is an electrical or an RF power. Thus we can easily identify that the powers of the distortion terms are proportional to the square of their amplitudes. So, we can deduce that the power of the HD2 terms expressed in decibels are approximately 6 dB lower compared to the IMD2 powers, and the HD3 powers are approximately 9.5 dB lower relative to the IMD3 powers. Therefore, we can affirm that

$$P_{\mathrm{HD2}} = P_{\mathrm{IMD2}} - 6\,\mathrm{dB}$$
$$P_{\mathrm{HD3}} = P_{\mathrm{IMD3}} - 9.5\,\mathrm{dB}. \quad (21)$$

Moreover, as we can observe in (19) and (20), all amplitudes are function of σ, so one can set to zero and cancel the desired nonlinearity with an optimum design parameter for this purpose. Therefore, the model provides a wide range of possibilities of linearization including all design parameters of the modulator. Also, since the model starts from the effective index change versus dc bias voltage, any difference in dimensions or diode doping profile respect to the design values due to fabrication variations will change the curve and will be taken into account.

B. Model Results

As it can be observed from the dependency of distortion amplitudes on the parameter σ in the obtained analytical expressions, the phase shifter length is a parameter which strongly affects the distortion. So, there will be an optimum phase shifter length which allows linearizing the modulator cancelling the third-order intermodulation product (dominant for less than one octave systems). For example, starting from a nonlinear effective index change curve as a function of dc bias voltage with $k = 0.52.10^{-3}$ and $V_b = 8$ V in (3), in a quadrature bias modulator (modulator is designed such that the bias phase shift between the two arms at $V_{\mathrm{DC}} = 0$ and $V_{\mathrm{RF}} = 0$ is $\pi/2$), one can linearize the modulator cancelling the third-order nonlinearity knowing the optimum phase shifter length. Fig. 1 shows the lengths of the phase shifter which yield the most linear performance for several dc voltages. It can be observed, for example, that for a dc voltage of 1 V the modulator phase shifter length must be 825.5 μm.

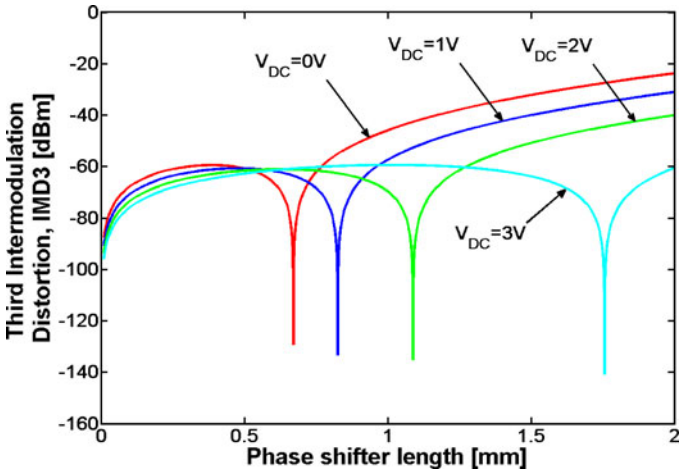

Fig. 1. Third-order intermodulation product power as a function of the phase shifter length in a $\Delta\Phi_{\mathrm{Bias}} = \pi/2$ modulator with a wavelength laser of 1550 nm.

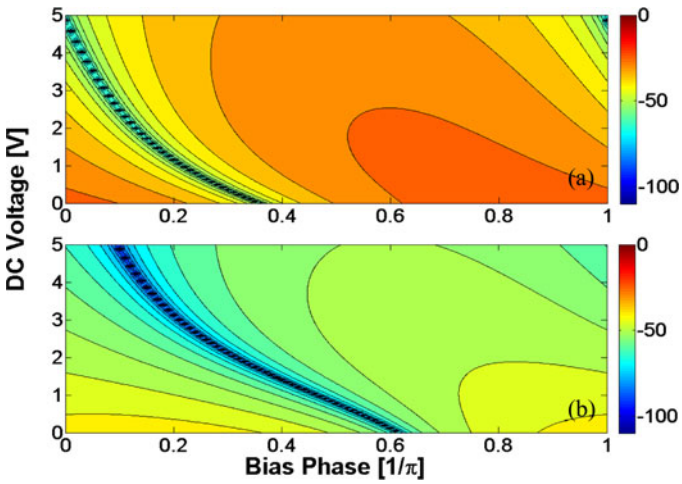

Fig. 2. (a) Contour of a second-order and (b) third-order intermodulation products power as a function of bias phase and dc bias voltage for an MZI with a phase shifter length of 1 mm and $\lambda = 1550$ nm.

Furthermore, as it can be deduced from (18), the nonlinearity of a silicon modulator also depends on the bias phase. Fig. 2 shows this dependency for a 1mm MZI phase shifter length. This figure represents a contour of the second-order (see Fig. 2(a)) and third-order (see Fig. 2(b)) intermodulation distortions, $\mathrm{P}_{\mathrm{IMD2}}$, and $\mathrm{P}_{\mathrm{IMD3}}$ respectively, as a function of the dc voltage and bias phase. For example, for 1 V of dc we can eliminate the third order term if the bias phase is 0.47π. In such case, the second-order intermodulation product would have a value of -26.54 dBm. In the same way, for 4V a bias phase shift of 0.15π would result in the third-order intermodulation term cancellation.

In order to corroborate our analytical model, we have performed a simulation in which the signal at the modulator output (time domain waveform) is converted to the frequency domain

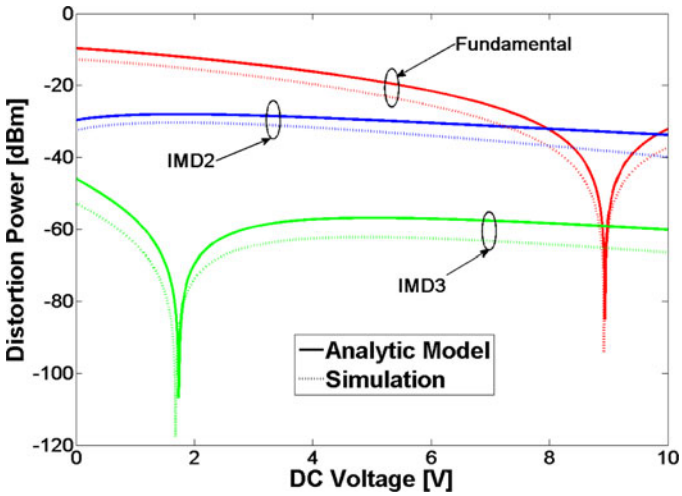

Fig. 3. Fundamental and intermodulation products power as a function of dc voltage in a fixed wavelength of 1550 nm for a 1 mm MZI under the condition $\Delta\Phi_{\mathrm{Bias}} = \pi/2$.

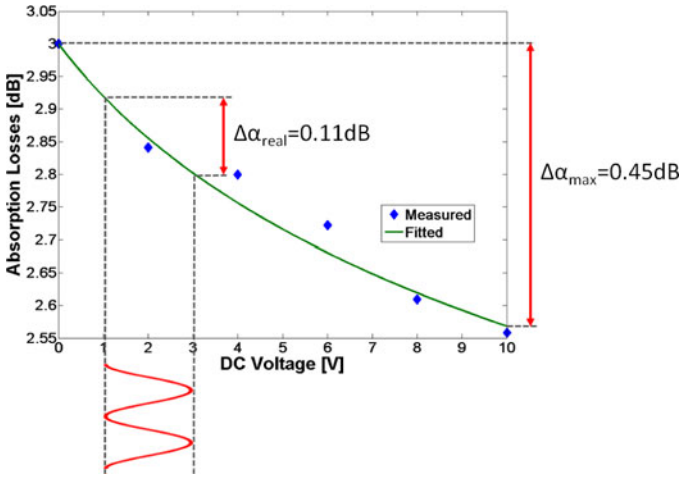

Fig. 4. Absorption losses variation with the dc voltage. The fitted curve is obtained from a logarithmic nonlinear approximation. It is shown both the maximum variation of absorption losses between 0 and 10 V and the absorption losses variation with the voltage for 2 V_{pp} of RF modulation voltage.

by performing a Fourier Fast Transfer (FFT). Then, one can select the desired frequency components and obtain its amplitude. This simulation allowed us to check the correct model performance since both simulation and analytic model show similar results. This can be observed in Fig. 3 where only some level error can be appreciated between simulation and our analytical model, but curves follow the same trend. In any case, the analytical expressions always overestimate the simulation results.

For a fixed quadrature modulator with an active length of 1 mm and a fixed 1550 nm wavelength, we can obtain from Fig. 3 that approximately 1.7 V is the optimum dc voltage for cancelling the third-order intermodulation term. Moreover we can observe in such Fig. 3 another point of view of the model application: for a dc voltage around 8.9 V the fundamental term vanishes and the second-order intermodulation product is maximized. This point could be useful for a frequency up-conversion process. The input signal can be set in the fundamental frequency and the signal information can be received in the second-order term ensuring a good level of power in such signal.

It should be noticed that the free carrier concentration variation due to the plasma dispersion effect alters the imaginary part of the refractive index thus introducing absorption losses in the material. Such absorption losses usually depend on the applied voltage in a nonlinear form, which also needs to be taken into account in the nonlinear distortion analysis.

First, the effect of constant optical losses in the arms of the MZI on the nonlinear distortion has been analyzed by means of simulations. It has been obtained that having an unbalanced power distribution at the arms of the MZI only affects to the absolute value of the RF output power but the transmission response remains unaltered so, quality parameters as CDR or SFDR are not affected.

On the other hand, the dependency of absorption losses with voltage can also be approximated by a logarithmic form. Simulation results show that in this case the transmission response of the intermodulation products is red-shifted with respect to

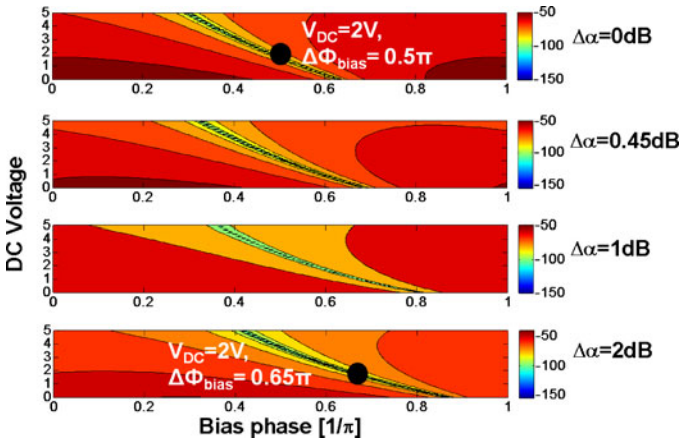

Fig. 5. RF output power of the IMD3 intermodulation product as a function of the bias phase and dc voltage for different values of absorption losses variation. The absorption losses compensation through Φ_{bias} parameter in a specific case for modulation linearization it is also shown.

the response obtained with the developed model, i.e. the case of having no loss. Therefore, the variation of absorption losses ($\Delta\alpha = \alpha_{\max} - \alpha_{\min}$) with voltage will reduce the accuracy of the model. However, the effect introduced by losses can be compensated in a real case by adjusting the bias (Φ_{bias}) for the target V_{DC}.

In the specific case of the 1 mm modulator under study in this study, the measured voltage-dependent absorption losses are very low so the effect is almost negligible. It has been obtained that the maximum variation is $\Delta\alpha = 0.45$ dB between 0 and 10 V, that is, for $\Delta V = 10$ V. So, if the RF modulation voltage is around 2 V_{pp}, the variation of absorption losses with voltage will be of the order of 0.11 dB, as shown in Fig. 4.

Fig. 5 shows the RF output power of the IMD3 intermodulation product as a function of the bias phase and dc voltage. It can be seen that the effect of losses are almost negligible for the case of $\Delta\alpha = 0.45$ dB but discrepancies are more noticeable as losses increases. However, if, for example, the IMD3 is

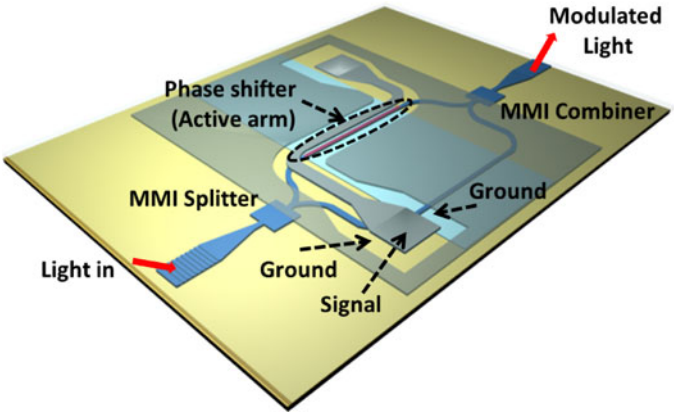

Fig. 6. Schematic of the fabricated silicon-based electro-optic MZI modulator. The MZI is asymmetric with a length difference of 180 μm and the phase shifter in the shorter arm is 1 mm of length. MMI are used for dividing the input light and combine the output modulated signal.

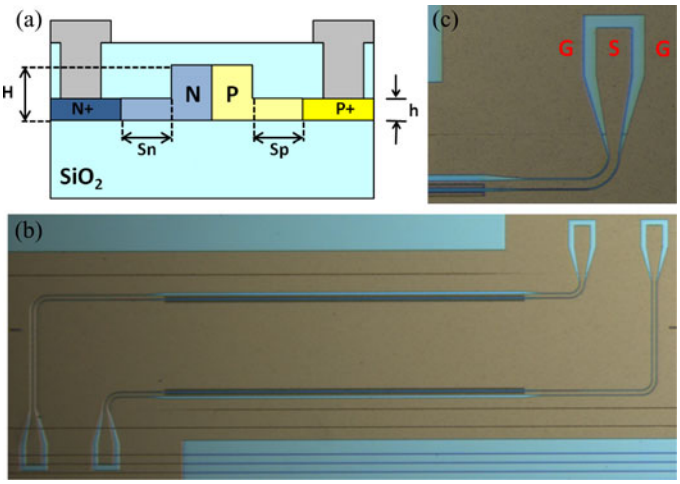

Fig. 7. (a) Schematic of the PN junction located at the middle of the active waveguide phase shifter, (b) optical microscope image of the fabricated modulator with a clear view of the traveling-wave ground–signal–ground (GSG) coplanar, electrodes, and (c) detail of the GSG electrode.

minimized for $V_{DC} = 2$ V and a $\Phi_{bias} = 0.5\pi$. The effect of losses could be compensated just by slightly increasing Φ_{bias} to 0.65π for a worst-case scenario of $\Delta\alpha = 2$ dB. Therefore, the developed model remains as a powerful tool for analyzing nonlinear distortion in silicon MZI modulators.

III. Model Validation

A. Fabricated Device Structure

The silicon-based modulator consists of an asymmetric MZI (as shown in Fig. 6) and the optical phase modulation is achieved by depleting the majority carriers from a reverse biased PN-junction located in the middle of the waveguide (see Fig. 7(a)) and embedded in the shorter arm of the MZI.

The length of the shorter arm (L_{ACT}) of the MZI is 1 mm and the length difference between both arms (ΔL) is 180μm with MMI coupler splitter and combiner in the input and output respectively. The silicon waveguides of dimensions of 220 nm $\times$ 460 nm have been partially dry etched to leave a

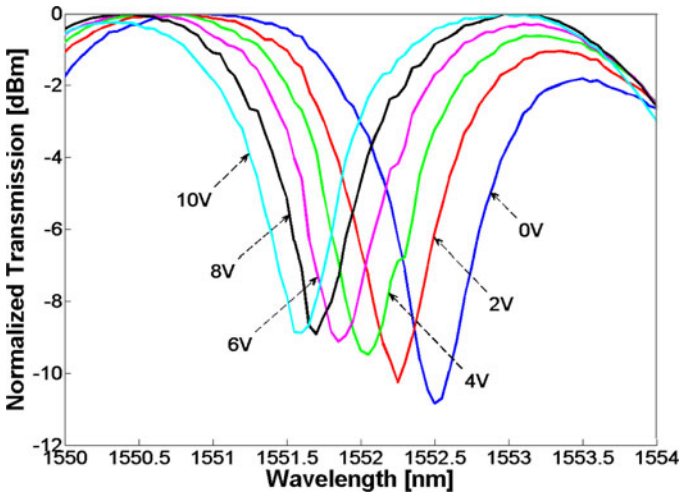

Fig. 8. Normalized dc transmission spectrum of the MZI modulator for different applied dc voltages.

100 nm thick slab. Doping concentrations in the p- and n-type regions of the diode are 4.10^{17} cm^{-3} and 5.10^{17} cm^{-3} respectively. The lumped electrode is formed by depositing a compound AlCu layer on top of the highly doped p^+ and n^+ regions with concentrations of 1.10^{20} cm^{-3} in order to obtain low resistive contacts. These are placed 450 nm and 500 nm for p^+ and n^+, respectively, away from the rib edges to minimize the overlap between the optical mode and therefore reduce optical losses. As can be observed from Fig. 6, the incoming coherent light is coupled vertically to the chip via grating couplers. A traveling-wave ground–signal–ground (GSG) coplanar design has been used to enable further high-speed radio-frequency measurements (see Fig. 7(b) and (c)). The complete fabrication process is described in [8].

As it was mentioned in the previous section, the model starts from the effective index change measurement, so, first of all, static and dc performance measurements have been carried out.

The spectrum of the silicon-based MZI exhibits a free-spectral range (*FSR*) of 2.42 nm and a 10 dB drop in transmission at the resonant wavelength around 1552 nm. Fig. 8 shows the MZI normalized transmission spectrum for varying dc voltages from 0 to 10 V.

As the modulator is asymmetric we have had to take into account this asymmetry in the bias phase as follows:

$$\Delta\Phi_{Bias} = \Phi_{Offset} - \Delta\Phi_{Asym.} \tag{22}$$

with:

$$\Delta\Phi_{Asym.} = \frac{2\pi}{\lambda} n_g \Delta L \tag{23}$$

where n_g is the group index and ΔL is the length difference between both MZI arms. Moreover, the minus sign is because the active area is located in the shorter arm and thus the resonance shifts to lower wavelengths with the dc voltage. Finally, we have added an offset term (Φ_{offset}) which is required to fit the theoretical spectrum with the experimental one (in dc measurements). So, for a fixed arm difference, the bias point of the modulator can be tuned either through acting on the dc voltage

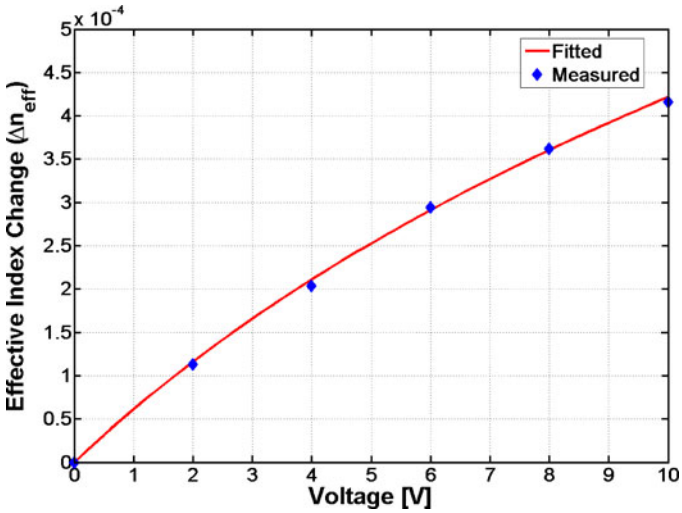

Fig. 9. Effective index change with the voltage. The measured data are obtained from the measured voltage-induced wavelength shift through equation (24). The fitted curve is obtained from nonlinear approximation described in (3).

or on the operation wavelength and vice versa. Taking into account (22) and (23) and plugging them into (18), one can obtain the optimum length difference and dc voltage for cancelling the desired intermodulation distortion. From the measured FSR, the group index has been calculated to be 3.9. On the other hand, the voltage-induced wavelength shift ($\Delta\lambda$) in the MZI modulator output spectrum and the index group can be used to extract the effective index variations ($\Delta_{n\text{eff}}$), through (24):

$$\Delta n_{\text{eff}} = \frac{\Delta\lambda}{\lambda} n_g \frac{\Delta L}{L_{\text{ACT}}}. \tag{24}$$

Fig. 9 depicts the calculated and fitted effective index variation as a function of applied dc voltage. The fitted curve has been obtained from the nonlinear approximation described in (3).

B. Experimental Validation

To validate the analytical model with experimental measurements we have performed a single-tone test and analyzed the harmonic distortion. The experimental set-up used for the RF analysis of the silicon-based electro-optic MZI modulator is shown in Fig. 10. The input light emitted by an External Cavity Laser (ECL) is coupled from standard single mode fibers to the chip via grating couplers. The polarization is optimized via the use of a polarization controller. One signal generator operating at f_{RF} is coupled to a DC voltage using a bias-Tee and applied through high speed GSG probes to one port of the silicon MZI modulator while the other port is terminated with a 50 Ω load. The output modulated signal is amplified with an erbium-doped fiber amplifier (EDFA), filtered by a tunable optical filter (OF) and split with a 50/50 optical splitter with the aim of photo-detecting and measuring the optical output by an optical power meter simultaneously. Finally, an electrical hybrid is used to separate the photo-detected signal to a vectorial signal analyzer for measuring the electrical received signal in

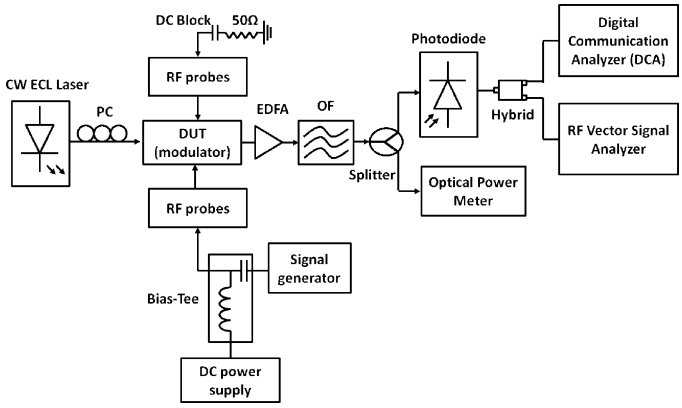

Fig. 10. Schematic of the experimental setup for the single-tone test carried out to experimental validation of the model.

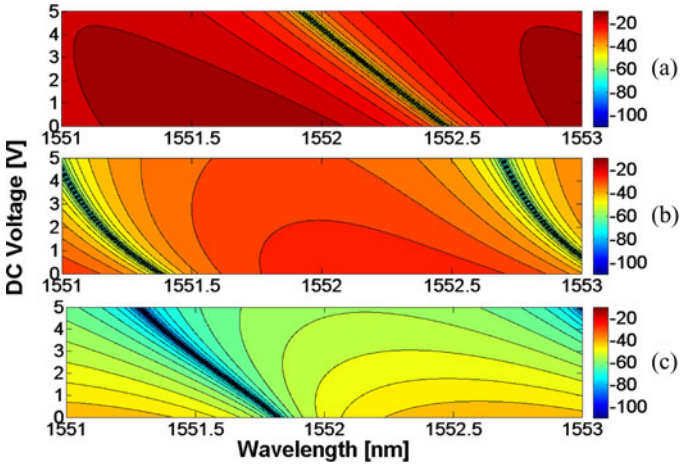

Fig. 11. (a) Contour of the fundamental, (b) the second and (c) the third-order harmonic products powers as a function of dc voltage and wavelength for our fabricated MZI.

terms of frequency and to a digital communication analyzer for measuring the temporal signals.

As mentioned previously, due to the asymmetric MZI structure and the material in the active area, the bias point of the modulator can be tuned either through acting on the dc voltage or on the operation wavelength in contrast with conventional $LiNbO_3$ modulators in which the bias point is driven only with a dc voltage. So, for a given wavelength, linear or nonlinear optimum operation can be achieved by adjusting the dc voltage and vice-versa. Thereby, representations of the distortion as a function of dc voltage and wavelength can help the designer to obtain the optimum combination wavelength-dc voltage point. Fig. 11 shows a contour of fundamental ($P_{\text{FUNDAM.}}$) in Fig. 11(a), second harmonic (P_{HD2}) in Fig. 11(b) and third harmonic (P_{HD3}) in Fig. 11(c), obtained from analytical expressions for our fabricated device. So, Fig. 11 shows that for 1V of V_{DC} the HD2 is minimized at around 1551.25 nm and HD3 at 1551.75 nm.

To validate these results, we first tested the model by measuring the harmonic distortion utilizing a fixed dc voltage of 1 V (see Fig. 12) and tuning the operating wavelength. As it can be observed in the figure below, the measurements show the same trends and are in very good agreement with the analytic

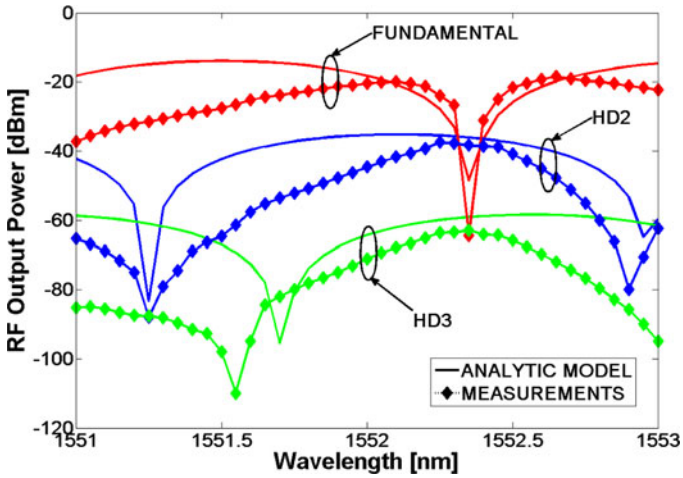

Fig. 12. Measured values and obtained curves from the analytical expressions of the fundamental and harmonic distortion performance as a function of the wavelength for a dc bias voltage of 1 V. The RF input power of the singletone is 10 dBm (2 V_{pp}).

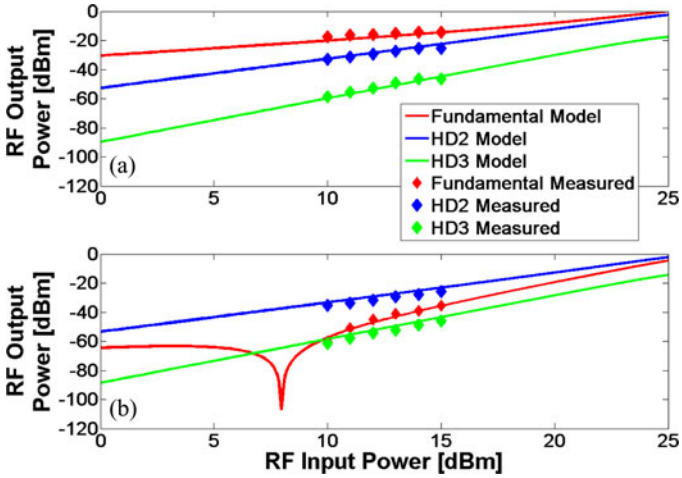

Fig. 14. Fundamental, HD2, and HD3 powers as a function of the modulating RF input power for (a) $\lambda = 1552.1$ nm and (b) $\lambda = 1552.4$ nm. Curves are obtained from the analytical model and VDC = 1 V.

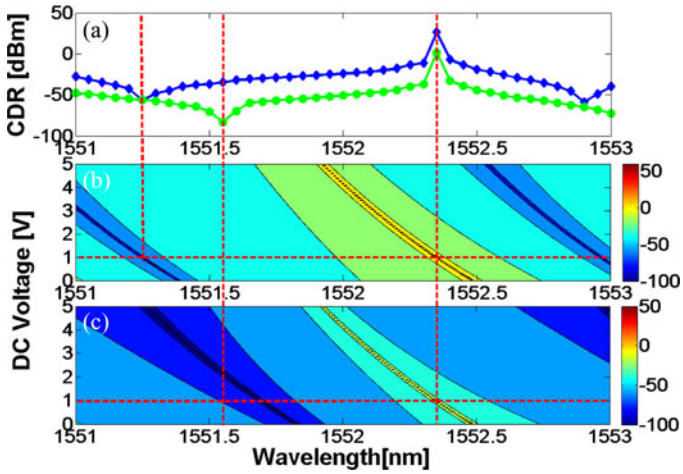

Fig. 13. Carrier-to-distortion ratio (a) from the experimental measurements and (b) CDR2 and (c) CDR3 from the analytical model. The RF input power of the single-tone is 10 dBm (2 V_{pp}).

model corroborating the results obtained from Fig. 11. A slight displacement of 0.2nm is produced in the HD3 term which is attributed to the characterization process. Moreover, it must be highlighted that the experimental curves are affected by the band-pass of the optical filter shape.

The level of distortion using the carrier-to-distortion parameter can also be evaluated. Defining it as the ratio between the harmonic distortion product power and the received power fundamental tone:

$$\mathrm{CDR}_2 = \frac{P_{\mathrm{HD2}}}{P_{\mathrm{FUNDAM.}}} \tag{25}$$

$$\mathrm{CDR}_3 = \frac{P_{\mathrm{HD3}}}{P_{\mathrm{FUNDAM.}}}. \tag{26}$$

Fig. 13 shows the experimental CDR (see Fig. 13(a)), theoretical CDR_2 (see Fig. 13(b)) and CDR_3 (see Fig. 13(c)) as a function of the wavelength for 1 V of dc voltage. From that figure we can see that according to the analytical expressions, for 1 V maximum CDR, around 20 dB for CDR_2 and around 1 dB for CDR_3, appears at 1552.4 nm as expected from Fig. 10 in which the fundamental is minimized. In contrast, minimum CDR, around –56 dB for CDR_2 and –83.5 dB for CDR_3 (obviously, the slight error displacement in HD3 appears again) are obtained at 1551.25 nm where HD2 is reduced and at 1551.55 nm where HD3 is reduced, respectively. So, we can affirm that the analytically estimated CDR is found to be in good agreement with the experimental one.

Another type of measurement consists of the electrical response of the harmonic distortion as a function of the RF input power and fixing the operating wavelength and dc voltage. These results are shown in Fig. 12 for 1 V of dc bias at $\lambda = 1552.1$ nm (see Fig. 14(a)) which is the wavelength where the measured fundamental signal is maximum and $\lambda = 1552.4$ nm (see Fig. 14(b)) where it is minimum. As it can be observed, the fitted curves obtained from the analytical model fit with the experimental data. For example, in 1552.4 nm for an input RF power of 10 dBm, the fundamental tone remains under HD2 more than 20 dB and at around the same level power of HD3 as expected from Fig. 12 and Fig. 13.

Finally, the modulation depth has been measured. It is well known that over-modulating a modulation device, which occurs when the RF modulating signal swing is too high, produces high distortion levels which strongly affect the signal output creating undesired harmonics. So, the modulation depth as a function of the RF input power has been obtained through the output temporal signals to corroborate that the measured harmonics in our fabricated device are only due to the modulator nonlinear feature and not due to over-modulation. This can be observed in Fig. 15 for $\lambda = 1552.1$ nm. No modulation depth higher than the unit is obtained in the whole range of RF input powers measured. Figure inset shows an example of the measured temporal signal. In particular it corresponds to the case of 12 dBm of RF input power which results in a modulation depth of around 50%.

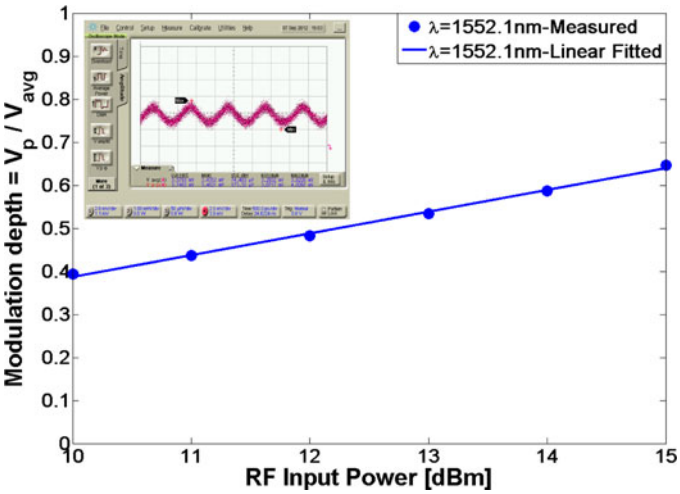

Fig. 15. Modulation depth as a function of the RF input power for the case of $\lambda = 1552.1$ nm and VDC $= 1$ V. It is observed that no over-modulation is produced.

IV. Conclusion

We have developed analytical expressions for the harmonic and intermodulation nonlinear distortions of a silicon-based electro-optic Mach-Zehnder Interferometer modulator due to the nonlinear feature of the silicon and the modulator transfer function. Distortion equations are estimated analytically and found to be in good agreement with numerical simulations. Some of the model applications have been shown as obtaining the optimal phase shifter length or length difference between the MZI arms for cancelling the third-order intermodulation distortion, allowing a linearized modulator. Finally, the harmonic distortion calculated by the analytical model has been validated by experimental results including the carrier-to-distortion parameter showing excellent matching between the model results and experimental data. Given the growing advantages of silicon photonics and therefore of silicon modulators for emerging RoF applications, this model gives a potential tool to predict the nonlinear modulator performance and the parameters needed for a full study of an analog photonic link.

References

[1] J. Capmany and D. Novak, "Microwave photonics combines two worlds," *Nat. Photon.*, vol. 1, no. 6, pp. 319–330, Jun. 2007.

[2] A. Seeds and K. Williams, "Microwave photonics," *J. Lightw. Technol.*, vol. 24, pp. 4628–4641, 2006.

[3] R. A. Soref, "The past, present, and future of silicon photonics," *IEEE J. Sel. Topics Quantum Electron.*, vol. 12, no. 6, pp. 1678–1687, Nov./Dec. 2006.

[4] B. Jalali and S. Fathpour, "Silicon photonics," *J. Lightw. Technol.*, vol. 24, no. 12, pp. 4600–4615, 2006.

[5] B. G. Lee, A. Biberman, J. Chan, and K. Bergman, "High-performance modulators and switches for silicon photonic networks-on-chip," *IEEE J. Sel. Topics Quantum Electron.*, vol. 16, no. 1, pp. 6–22, Jan./ Feb. 2010.

[6] G. T. Reed, G. Mashanovich, F. Y. Gardes, and D. J. Thomson, "Silicon optical modulators," *Nat. Photon.*, vol. 4, no. 8, pp. 518–526, 2010.

[7] R. Soref and B. Bennett, "Electrooptical effects in silicon," *IEEE J. Sel. Topics Quantum Electron*, vol. 23, no. 1, pp. 123–129, Jan. 1987.

[8] A. Brimont, A. M. Gutierrez, M. Aamer, D. J. Thomson, F. Y. Gardes, J. Fedeli, G. T. Reed, J. Marti, and P. Sanchis, "Slow-light-enhanced silicon optical modulators under low-drive-voltage operation," *IEEE J. Photon*, vol. 4, no. 5, pp. 1306–1315, Oct. 2012.

[9] F. Gardes, D. Thomson, N. Emerson, and G. Reed, "40 Gb/s silicon photonics modulator for TE and TM polarisations," *Opt. Exp.*, vol. 19, pp. 11804–11814, 2011.

[10] D. J. Thomson, F. Y. Gardes, J.-M. Fedeli, S. Zlatanovic, H. Youfang, B. P. P. Kuo, E. Myslivets, N. Alic, S. Radic, G. Z. Mashanovich, and G. T. Reed, "50-Gb/s Silicon Optical Modulator," *IEEE Photon. Technol. Lett.*, vol. 24, no. 4, pp. 234–236, Feb. 2012.

[11] A. Brimont, D. J. Thomson, F. Y. Gardes, J-M. Fedeli, G. T. Reed, J. Marti, and P. Sanchis, "Low drive voltage 10 Gb/s and high contrast 40 Gb/s silicon slow wave modulators," in *Proc. IEEE 9th Int. Conf. Group IV Photon. (GFP)*, Aug. 29–31, 2012, pp. 195–197.

[12] W. Green, M. Rooks, L. Sekaric, and Y. Vlasov, "Ultra-compact, low RF power, 10 Gb/s siliconMach-Zehnder modulator," *Opt. Exp.*, vol. 15, pp. 17106–17113, 2007.

[13] S. Akiyama, T. Baba, M. Imai, T. Akagawa, M. Takahashi, N. Hirayama, H. Takahashi, Y. Noguchi, H. Okayama, T. Horikawa, and T. Usuki, "12.5-Gb/s operation with 0.29-V·cm VπLπ using silicon Mach-Zehnder modulator based-on forward-biased pin diode," *Opt. Exp.*, vol. 20, pp. 2911–2923, 2012.

[14] L. Liao, A. Liu, J. Basak, H. Nguyen, M. Paniccia, D. Rubin, Y. Chetrit, R. Cohen, and N. Izhaky, "40 Gbit/s silicon optical modulator for high-speed applications," *Electron. Lett.*, vol. 43, no. 22, 2007.

[15] M. Ziebell, D. Marris-Morini, G. Rasigade, J. Fédéli, P. Crozat, E. Cassan, D. Bouville, and L. Vivien, "40 Gbit/s low-loss silicon optical modulator based on a pin diode," *Opt. Exp.*, vol. 20, pp. 10591–10596, 2012.

[16] J. Ding, H. Chen, L. Yang, L. Zhang, R. Ji, Y. Tian, W. Zhu, Y. Lu, P. Zhou, R. Min, and M. Yu, "Ultra-low-power carrier-depletion Mach-Zehnder silicon optical modulator," *Opt. Exp.*, vol. 20, pp. 7081–7087, 2012.

[17] S. Manipatruni, X. Qianfan, B. Schmidt, J. Shakya, and M. Lipson, "High Speed carrier injection 18 Gb/s silicon micro-ring electro-optic Modulator," in *Proc. 20th Annual Meeting of the IEEE Lasers and Electro-Optics Society*, 2007, pp. 537–538.

[18] P. Dong, S. Liao, H. Liang, W. Qian, X. Wang, R. Shafiiha, D. Feng, G. Li, X. Zheng, A. Krishnamoorthy, and M. Asghari, "High-speed and compact silicon modulator based on a racetrack resonator with a 1 V drive voltage," *Opt. Letts.*, vol. 35, pp. 3246–3248, 2010.

[19] G. Li, X. Zheng, J. Yao, H. Thacker, I. Shubin, Y. Luo, J. E. Cunningham, and A. V. Krishnamoorthy, "25Gb/s 1 V-driving CMOS ring modulator with integrated thermal tuning," *Opt. Exp.*, vol. 19, no. 21, pp. 20435–20443, 2011.

[20] A. Brimont, D. Thomson, F. Gardes, J. Fedeli, G. Reed, J. Martí, and P. Sanchis, "High-contrast 40Gb/s operation of a 500μm long silicon carrier-depletion slow wave modulator," *Opt. Lett.*, vol. 37, pp. 3504–3506, 2012.

[21] W. B. Bridges and J. H. Schaffner, "Distortion in linearized electrooptic modulators," *IEEE Trans. Microw. Theory Tech.*, vol. 43, no. 9, pp. 2184–2197, Sep. 1995.

[22] A. Karim and J. Devenport, "Low noise figure microwave photonic link," in *Proc. IEEE /MTT-S Int. Microw. Symp.*, Jun. 3–8 2007, pp. 1519–1522.

[23] G. Zhang, X. Zheng, S. Li, H. Zhang, and B. Zhou, "Postcompensation for nonlinearity of Mach-Zehnder modulator in radio-over-fiber system based on second-order optical sideband processing," *Opt. Lett.*, vol. 37, pp. 806–808, 2012.

[24] A. Khilo, C. Sorace, and F. Kärtner, "Broadband linearized silicon modulator," *Opt. Exp.*, vol. 19, pp. 4485–4500, 2011.

[25] F. Vacondio, M. Mirshafiei, J. Basak, L. Ansheng, L. Ling, M. Paniccia, and L. A. Rusch, "A silicon modulator enabling RF over fiber for 802.11 OFDM signals," *IEEE J. Sel. Topics Quantum Electron.*, vol. 16, no. 1, pp. 141–148, Jan./Feb. 2010.

[26] S. Muping, Z. Lin, R. G. Beausoleil, and A. E. Willner, "Nonlinear distortion in a silicon microring-based electro-optic modulator for analog optical links," *IEEE J. Sel. Topics Quantum Electron.*, vol. 16, no. 1, pp. 185–191, Jan./Feb. 2010.

[27] J. Marti, V. Polo, F. Ramos, and J. M. Fuster, "Single Mach–Zehnder modulator electro-optical harmonic mixer for broadband microwave/millimetre-wave applications," *Wireless Personal Commun.*, vol. 15, pp. 31–42, 2000.

[28] B. Cabon, "Microwave photonic mixing," *Trans. Comput. Sci. Eng. Electr. Eng.*, vol. 17, p. 13, 2010.

[29] G. K. Gopalakrishnan, W. K. Burns, and C. H. Bulmer, "Microwave-optical mixing in LiNbO3 modulators," *IEEE Trans. Microw. Theory Techn.*, vol. 41, no. 12, pp. 2383–2391, Dec. 1993.

[30] A. Karim and J. Devenport, "High dynamic range microwave photonic links for RF signal transport and RF-IF conversion," *J. Lightw.Technol.*, vol. 26, no. 15, pp. 2718–2724, Aug. 1, 2008.
[31] V. Pagán, B. Haas, and T. Murphy, "Linearized electrooptic microwave downconversion using phase modulation and optical filtering," *Opt. Exp.*, vol. 19, pp. 883–895, 2011.
[32] A. Gutiérrez, A. Brimont, J. Herrera, M. Aamer, J. Martí, D. Thomson, F. Gardes, G. Reed, J. Fedeli, and P. Sanchis, "Silicon slow-light-based photonic mixer for microwave-frequency conversion applications," *Opt. Lett.*, vol. 37, pp. 1721–1723, 2012.
[33] D. Marpaung, "High dynamic range analog photonic links design and implementation," M.S. Thesis, University of Twente, Enschede, The Netherlands, 2009.
[34] S. L. Chuang, *Physics of Optoelectronic Devices*. New York, NY, USA: Wiley, 1995.

Ana M. Gutiérrez was born in Valencia, Spain, in 1983. She received the Telecommunication Engineering degree from the Universitat Politecnica de Valencia as well as the Master's degree in technologies, systems, and communications networks, where she is working toward the Ph.D. degree from the Nanophotonics Technology Center. Her research interests include modeling and characterization of high-speed silicon modulator for both analog and digital applications.

Antoine Brimont was born in Valence, France, in 1982. He received the Engineering Master's degree in materials science and nanotechnology (M.Sc.) from the Institut National des Sciences Appliquées (INSA) de Rennes, France, as well as the Diplôme d'Études Approfondies (DEA) in physics from the Université de Rennes 1, France, in 2005. He also received the Diploma de Estudios Avanzados (DEA) as well as the Ph.D. in telecommunications engineering from the Universitat Politècnica de València, Spain, in 2008 and 2011, respectively. He is currently working as a Postdoctoral Researcher at the Valencia Nanophotonics Technology Center, Spain. His research interests include active and passive silicon photonic devices and specifically high-speed silicon modulators enhanced via slow light propagation. He has authored or coauthored more than 35 papers in peer-reviewed international journals and international conferences.

Javier Herrera received the Telecommunication Engineering degree and Telecommunication Engineer Ph.D. degree from Universitat Politècnica de València, in 2000 and 2005, respectively, where he joined the Nanophotonics Technology Center, as a Junior Research Engineer. In 2006, he joined the COBRA Research Institute, Eindhoven University of Technology as a Senior Research Engineer, returning to Nanophotonics Technology Center at 2008 as a Senior Research Engineer. He has been involved in several research projects funded by the European Comission related to fiber-optics, photonics, and broadband wireless systems and technologies such as IST-OBANET, ICT-LASAGNE, ICT-GANDALF, ICT-EUROFOS and ICT-FIVER. He has coauthored more than 80 journal and conference papers related to these technologies. In 2010, he joined FIBERNOVA SYSTEMS S. L. as an R&D engineer.

Mariam Aamer was born in Tangier, Morocco in 1982. She received the Telecommunication Engineering degree from the Universitat Politecnica de Valencia as well as the Master degree in technologies, systems, and communications networks, where she is currently working toward the Ph.D. degree in the Nanophotonics Technology Center. Her research interests include silicon photonic devices as rotator and splitter, as well as the development of transceiver for access networks in silicon photonics.

Dave J. Thomson is a senior Research Fellow in the Optoelectronics Research Centre (ORC), University of Southampton. His research interests include optical modulation, optical switching, integration, and packaging in silicon. He started his silicon photonics research in 2004 as a Ph.D. student at the University of Surrey under the guidance of Prof. G. Reed. His Ph.D. project involved investigating silicon-based total internal reflection optical switches and more specifically methods of restricting free carrier diffusion within such devices. In 2008, he took up a role as a Research Fellow in the same research group leading the work package on silicon optical modulators within the largest European silicon photonics project named HELIOS. Within this project, he designed the first silicon optical modulator operating at 50 Gbit/s. In 2011, he presented invited talks at SPIE Photonics West and IEEE Group IV Photonics conferences and in 2012 was selected to present his work at the SET for Britain event in the Houses of Parliament.

Frederic Y. Gardes is an Academic Fellow appointed as a Lecturer in the Department of Electronics and computer science (ECS), University of Southampton; he is conducting his research as part of the Optoelectronics Research Centre (ORC). His previous research covers silicon photonics and particularly high-speed active optical devices in silicon and germanium. In 2005, he initiated work on silicon optical depletion modulators and was the first to predict operation above 40 GHz. In 2011, he and his collaborators demonstrated optical modulation of up 50 Gb/s and a 40 Gb/s modulator with a quadrature extinction ratio (ER) of 10 dB setting a new state-of-the-art performance in both speed of modulation in silicon devices and extinction ratio. He is currently working with several national and international collaborators in two large research programs, where he leads the research effort in optical modulators and detector integration. These programs are the £5M U.K. Silicon Photonics project funded by EPSRC, and the £8M EU FP7 HELIOS. He is also involved in photonic crystal slow light, ultra-low power nano-cavity modulators, silicon/germanium QCSE devices, germanium and defect-induced detectors in silicon and active device integration in group IV materials. He has authored more than 80 publications and 5 book chapters in the field of silicon photonics. He has also been involved in the FP6 ePIXnet program and is a regular invited and contributing author to the major silicon photonics conferences around the world. He is also a member of the programme committee of the IEEE Group IV Photonics conference.

Graham T. **Reed** is a Professor of silicon photonics and a Group Leader. He has recently joined Southampton from the University of Surrey, where he was a Professor of optoelectronics, and was the Head of the Department of Electronic Engineering from 2006 to 2012. He is a pioneer in the field of silicon photonics, and acknowledged as the individual who initiated the research field in the U.K. He established the Silicon Photonics Research Group at Surrey in 1989. The first Silicon Photonics company in the world, Bookham Technology Inc., was founded by Reed's Ph.D. student, Dr. Rickman, and adopted the research developed in the Group. The Silicon Photonics Group has provided a series of world leading results since its inception, and are particularly well known for their work on silicon optical modulators. For example, the Group produced the first published design of an optical modulator with a bandwidth exceeding 1 GHz, and were the first to publish the design of a depletion mode optical modulator, which is now a technology standard device. More recently the team were responsible for the first all-silicon optical modulator operating at 40 Gb/s with a high extinction ratio (10 dB), as well as a second modulator design (also operating at 40 Gb/s) that operates close to polarization independence. They have now reported the first device operating at 50 Gb/s. He is a regular invited and contributing author to the major silicon photonics conferences around the world. He has served on numerous international conference committees, and has also chaired many others. To name but two, he has been the Cochair, of the silicon photonics symposium at Photonics West since it was first established in 2006, and in 2011 he was the Cochair of the prestigious silicon photonics conference, IEEE Group IV Photonics, held at the Royal Society in London. He is currently a member of five international conference committees, and has published more than 250 papers in the field of silicon photonics. He Co-chaired four international symposia/conferences in 2012.

Jean-Marc Fedeli received the Electronics Engineer Diploma from INPG Grenoble in 1978. Then, he conducted research work at the CEA-LETI on various magnetic memories and magnetic components as a Project Leader, Group Leader, and Program Manager. For two years, he acted as an Advanced Program Director in Memscap company for the development of RF-MEMS, then he returned to CEA-LETI in 2002 as a Coordinator of silicon photonic projects up to 2012. Under a large partnership with universities and research laboratories, he works on various technological aspects on photonics on CMOS (Si rib and stripe waveguides, Si3N4 and a-Si waveguides, slot waveguides), Si modulators, Ge photodetectors, and InP sources on Si. His main focus was on the integration of a photonic layer at the metallization level of an electronic circuit. He has been participating on different European FP6 projects (PICMOS, PHOLOGIC, MNTE, ePIXnet). Under the European FP7, he was involved in the WADIMOS, PhotonFAB (ePIXfab) projects and was a Program Manager of the HELIOS project. He is currently managing the FP7 PLAT4M project on Silicon Photonics Platform and involved in industrial projects on Silicon Photonics.

Pablo Sanchis received the Ingeniero de Telecomunicación degree (M.Sc.) and the Doctor Ingeniero de Telecomunicación degree (Ph.D.) from the Universidad Politécnica de Valencia, Valencia, Spain, in 2001 and 2005, respectively. He is a full-time Associate Professor at the Universidad Politécnica de Valencia and the Group Leader at the Valencia Nanophotonics Technology Centre. His research interests include modeling, design, and fabrication issues in integrated optics, especially in the field of silicon photonics. One of his main activities in the last years has been the enhancement of silicon photonics modulators via innovative and disruptive approaches. In 2011, his team demonstrated for the first time a 40 Gbit/s silicon carrier-depletion modulator enhanced via slow light propagation. He has been involved in several national research projects, some of them as a Principal Investigator, and European research projects with a growing responsibility and leadership (IST-2000-25390 OBANET, IST-017158-PHOLOGIC, NoE-004525 ePIXnet, IST-224312 HELIOS). He has authored more than 48 papers in peer-reviewed international journals and more than 90 papers in international conferences and he holds 4 patents.